Title: Climate drives spatial variation in Zika epidemics in Latin America

Mallory Harris[1], Jamie M. Caldwell[2*], Erin A. Mordecai[2]

1. Odum School of Ecology, University of Georgia, 140 E Green St, Athens, GA 30602
2. Biology Department, Stanford University, 371 Serra Mall, Stanford, CA, USA

* contact: jamie.sziklay@gmail.com

Keywords: Zika, force of infection, tSIR

Abstract

Between 2015 and 2017, Zika virus spread rapidly through populations in the Americas with no prior exposure to the disease. Although climate is a known determinant of many *Aedes*-transmitted diseases, it is currently unclear whether climate was a major driver the of Zika epidemic and how climate might have differentially impacted outbreak intensity across locations within Latin America. Here, we estimated force of infection for Zika over time and across provinces in Latin America using a time-varying Susceptible Infectious Recovered model. Climate factors explained less than 5% of the variation in weekly transmission intensity in a spatiotemporal model of force of infection by province over time, suggesting that week to week transmission within provinces may be too stochastic to predict. By contrast, climate and population factors were highly predictive of spatial variation in the presence and intensity of Zika transmission among provinces, with pseudo R^2 values between 0.33 and 0.60. Temperature, temperature range, rainfall, and population size were the most important predictors of where Zika transmission occurred, while rainfall, relative humidity, and a nonlinear effect of temperature were the best predictors of Zika intensity and burden. Surprisingly, force of infection was greatest in locations with temperatures near 24°C, much lower than previous estimates from mechanistic models, potentially suggesting that existing vector control programs and/or prior exposure to other mosquito-borne diseases may have limited transmission in locations most suitable for *Aedes aegypti*, the main vector of Zika, dengue, and chikungunya viruses in Latin America.

Introduction

The emergence and re-emergence of mosquito-borne diseases presents a global public health concern, yet trends in mosquito-borne disease transmission are hard to predict because they are influenced by the underlying immunity in the population, which is usually unknown [1–3]. The emergence and spread of Zika virus through Latin America in a population with no prior exposure or immunity to the disease provides an opportunity to characterize relationships among the environment, populations, and disease transmission without the confounding effects of pre-existing immunity (although cross-reactivity between dengue antibodies and Zika virus may provide some protection) [4]. Between 2015 and 2017, Zika rapidly spread to 51 countries and territories in the Americas, with over 800,000 cases reported [5]. Here, we quantified the force of infection for Zika and studied factors that contributed to variation in transmission across time and space as Zika emerged.

Force of infection, or the per capita rate at which susceptible individuals contract an infection, can be used to compare disease transmission over the course of an outbreak and across geographic regions [2,6]. Force of infection estimates can account for variation in the number of immune individuals and entomological factors that influence the time it takes for mosquito-borne diseases to be transmitted [2,6]. It can take up to several weeks for mosquitoes to spread diseases because transmission requires a mosquito to bite an infectious person, the pathogen to replicate and disseminate in the mosquito (during the extrinsic incubation period), and the mosquito to bite and infect a susceptible person [2,7–9]. Force of infection can be calculated over time to study how transmission rate changes over the course of an outbreak and to compare outbreaks of the same disease in different places [2,6,10–12].

The progression of an epidemic can be characterized and compared through measures of burden, intensity, and transmission rate [13,14]. We can quantitatively differentiate between epidemics with sharp peaks in case incidence that quickly burn through the susceptible population and more sustained, low-level transmission [6,15,16]. Instances when high case incidence coincides with a low force of infection may indicate the presence of imported cases [17]. Each of these epidemic metrics may be affected to a different extent by climate and population factors, in addition to country and province-level features like existing transportation infrastructure and vector control resources [4,9,18,19]. Additionally, conditions that enable the establishment of a disease may differ from those that drive higher epidemic intensity following establishment [20].

Climate is a key determinant for whether mosquito-borne disease transmission can occur and the intensity of outbreaks because of its effects on vector dynamics. The primary vector of Zika in Latin America is *Aedes aegypti*, which also spreads chikungunya and dengue viruses [21]. Disease transmission can only occur if climate conditions are suitable for pathogen and vector survival and reproduction, while the intensity of transmission may be affected by how close humidity, temperature, and rainfall are to optimal climate conditions for vector and pathogen performance [2,9,22–27]. Humidity is positively associated with mosquito survival [23]. Temperature influences mosquito fecundity, development, and survival, as well as factors contributing directly to transmission, including the extrinsic incubation period and mosquito biting rate [9,24,27–29]. These thermal responses are nonlinear with optimal disease transmission expected at 29°C for viruses transmitted by *A. aegypti* based on mechanistic models parameterized from laboratory experiments [20,25]. Mosquitoes require water to complete their life cycle and breed, but the relationship between mosquito abundance and rainfall is variable

[30–36]. The most notable reasons for this varying relationship are associated with extreme conditions, such as heavy rainfall that can kill and wash away larvae [37,38], and drought, which in certain regions promotes humans storing water in open containers that serve as breeding habitats [35,36]. Understanding how climate drives the emergence and intensity of Zika will be important for identifying regions where the disease is likely to become endemic, and, more generally, for predicting the potential trajectories of other mosquito-borne diseases that could emerge and re-emerge in the future, such as o'nyong nyong, Mayaro, and yellow fever [1,19,39–41].

In this study, we estimate weekly force of infection for Zika from human case reports across Latin America to examine the role of climate in driving the emergence and intensity of the 2015 to 2017 outbreak. Specifically, we use the models to ask how climate and population variation affect (1) when and where epidemics occur, (2) epidemic dynamics over time, and (3) geographic variation in the intensity of epidemics. We use disease case reports and force of infection estimates in two modeling frameworks. First, we examine variation in force of infection over time within provinces to understand how strongly climate predicts the probability of weekly local transmission and the intensity of weekly force of infection. Then, we examine spatial variation in several epidemic metrics, including total human cases and mean force of infection, to understand how climate and population factors shape epidemics geographically.

Materials and Methods

Epidemiological Data

To investigate Zika transmission dynamics over time and space in Latin America, we downloaded and preprocessed publicly available human case data. We used weekly suspected

115 and confirmed Zika cases between November 2015 and November 2017 for 156 provinces
116 across seven countries in Latin America (Colombia = 32 provinces, Dominican Republic = 32
117 provinces, Ecuador = 24 provinces, El Salvador = 14 provinces, Guatemala = 22 provinces, and
118 Mexico = 32 provinces) from the Centers for Disease Control and Prevention (CDC) Zika Data
119 Repository, which includes epidemiological bulletins provided by each country's ministry of
120 health [42]. We excluded fourteen provinces with fewer than ten weeks of case reporting or
121 irregular reporting intervals, because those provinces provided insufficient data to observe
122 meaningful trends in transmission (excluded provinces: Ecuador = eight provinces, Guatemala =
123 two provinces, and Mexico = four provinces). For the remaining provinces, we temporally
124 interpolated case data for weeks with missing data and reporting errors by averaging cases from
125 the weeks immediately preceding and following these intervals.
126
127 *Weather Data*
128 To investigate the effects of climate on Zika transmission, we downloaded weather data
129 and calculated climate metrics with time lags relevant to diseases spread by the *Aedes aegypti*
130 vector. We downloaded daily mean relative humidity, total rainfall, and mean, minimum, and
131 maximum temperatures from Weather Underground [43]. For each province, we used the
132 weather station nearest to the province's centroid that had the most complete climate record in
133 the timespan corresponding to the case data. We excluded from our analyses an additional fifteen
134 provinces that had no nearby weather station reporting in the desired time period (excluded
135 provinces: Colombia = six provinces, Dominican Republic = one province, Ecuador = two
136 provinces, El Salvador = two provinces, Guatemala = two provinces, and Mexico = two
137 provinces), and further excluded 277 weeks with mean temperatures outside of the range of 0-

138 40°C and rainfall values exceeding 250mm, as these extreme values are likely to be weather
139 station errors. Our analyses included the remaining 127 provinces with a total of 7,109 weekly
140 observations of epidemiological and weather data. We believe weather station data provides
141 more accurate measurements of climate near populated areas (as weather stations are located at
142 airports or operated for personal use) compared with modeled weather data such as the NOAA
143 National Centers for Environmental Prediction Reanalysis data (NCEP; see Figure S1 for a
144 comparison between data from Weather Underground and NCEP, a gridded global model based
145 on satellite data), and therefore chose to conduct our analyses with weather station data with a
146 reduced sample size due to missing weather stations in some provinces.

147 To investigate the spatiotemporal dynamics of transmission, we calculated lagged climate
148 metrics (see Figure S2 for heatmaps showing variation in climate by province over time), as
149 humidity, temperature, and rainfall influence transmission at a delay, which is commonly
150 assumed to be between one and two months [30–32,34,35,44]. Specifically, we calculated
151 humidity, mean temperature, and temperature range (difference between the maximum and
152 minimum temperatures observed) over a three-week period, lagged by six weeks from the week
153 of case reporting (i.e., nine to seven weeks prior, following previous work) [20,45,46]. Similarly,
154 we calculated the cumulative rainfall over a six-week period, lagged by three weeks from the
155 week of case reporting (i.e., nine to four weeks prior), extending the window applied to lagged
156 temperature period by three weeks in order to better capture the effects of water accumulation
157 over time [47,48]. To compare differences in overall epidemic characteristics (e.g., total number
158 of cases, mean force of infection Table 1; Figure 1) among provinces, we also calculated
159 province-level mean humidity, mean temperature, temperature range, and cumulative rainfall
160 over the biologically relevant time lag described above.

tSIR Model

We estimated weekly force of infection by fitting time-varying Susceptible Infectious Recovered (tSIR) models to the human case data [42]. We assumed a static population size because the human population did not change significantly over the course of the epidemic, and we assumed that Zika was introduced to a fully susceptible population since it had never been documented before in this region. Therefore, we set the initial susceptible population (S_0) as the most recent estimate of population (N) available from *City Population* as of June 2017, and modeled the susceptible population following Zika introduction as $S_t = S_{t-1} - I_t$ where S indicates the susceptible population at time (t) or $(t-1)$ and I indicates the infected population at time (t) [49]. We defined effective infectious individuals based on the modification of the tSIR model for vector-borne diseases developed by Perkins et al. 2015 for chikungunya transmission because of similarities in the transmission ecology of their shared vector [2,34]. Using the infectious periods derived for chikungunya, we assumed that humans can transmit the parasite to mosquitoes for five days after reporting symptoms and that secondary human infections can arise from primary cases reported one to five weeks prior [50]. We calculated the effective number of infectious individuals ($\tilde{I}_t$) as a weighted sum of infectious individuals (I_{t-n}) within a five-week serial interval (k=5). We used the same methods as the Perkins et al. 2015 model for chikungunya transmission to solve for the weights (ω_n) and substituted the appropriate serial interval distribution for Zika (a Gaussian distribution with mean 20 days and standard deviation 7.4 days) [2,51,52]:

$$\tilde{I}_t = \sum_{n=1}^{k} \omega_n I_{t-n} \tag{1}$$

Individuals entered the recovered class after the five-week serial interval. We fit tSIR models to case data for each province to calculate time-varying force of infection (β_t):

$$I_t = \beta_t \frac{\tilde{I}_t^{\alpha}}{N} S_{t-1} \tag{2}$$

Here, the mixing parameter α indicates homogeneous frequency-dependent contact rate between cases in each province. We fixed the mixing parameter due to the tradeoff between capturing heterogeneity in transmission or mixing, a method commonly used in tSIR studies focused on transmission dynamics [10,53–56]. Given the similar transmission dynamics of chikungunya and Zika, we set the mixing parameter equal to 0.74, the value for chikungunya calculated in the Perkins et al. study [2,51]. By rearranging equation 2, we solved for $\ln(\beta_t)$ using the following equation:

$$\ln(\beta_t) = \ln(I_t) + \ln(N) - \ln(S_{t-1}) - \alpha \ln(\tilde{I}_t) \tag{3}$$

Spatiotemporal Model

We investigated how strongly climate predicts the probability of weekly local transmission and the intensity of weekly force of infection by regressing force of infection against biologically relevant lagged and normalized climate factors. Since the transmission parameters (β_t) were zero-inflated, we fit a two-step hurdle model that first predicts the probability that the force of infection, β_{it}, will exceed zero in a given province (i) and week (t) (i.e., presence of local transmission), and then predicts the magnitude of logged force of infection, $\ln(\beta_{it})$ (i.e., intensity), given that β_t exceeds zero. To capture nonlinear relationships between transmission and temperature, we included a squared term for temperature [2,9,20].

We performed stepwise model selection using backward elimination, selecting the best fit models for both steps of the hurdle model as those with the highest adjusted R^2, and further constraining the selection process to prohibit models that include a nonlinear temperature term without a linear temperature term. To account for autocorrelation between observations within each province over time, we fit panel models with a two-way random effect:

$$Step\ 1\ -\ Presence/Absence: P(\beta_{it} > 0) \sim cx_{it} + \mu_i + \eta_t + \varepsilon_{it} \quad (4)$$

$$Step\ 2\ -\ Intensity\ Given\ Presence: ln(\beta_{it}) \sim cx_{it} + \mu_i + \eta_t + \varepsilon_{it} \quad (5)$$

The hurdle models include climate covariates (x), their corresponding coefficients (c), time-independent province random effect (μ), province-independent random effect of week (η), and an observation-specific error term (ε) accounting for time (t) and province (i). Regressions were conducted in R statistical software version 3.4.3 using the plm function in the plm package [57]. We also fit alternative fixed effect spatiotemporal models with month or month nested in province fixed effects (Table S3-4).

Spatial Models

We examined the factors that drove broad-scale geographic differences in Zika transmission by using linear regressions to compare epidemic metrics with normalized climate and population factors. The response variables included epidemic metrics based on incidence and force of infection (presence of local transmission, logged maximum force of infection, logged average force of infection, cumulative cases, and mean weekly cases), where each response variable was aggregated to a single value per province (Table 1; Figure 1). To account for additional variation among countries beyond climate and population factors, we included country as a fixed effect. Since some countries had local transmission in all provinces, we included

country as a random effect in the spatial model for the probability of local transmission in a given province. For the population factor, we used the number of people living in the largest city in each province based on census results and official estimates as of June 2017 downloaded from *City Population* [49]. The mean value of each lagged climate covariate was taken for each province across the time that cases were reported. For each spatial model, we performed stepwise model selection using backwards elimination, selecting the best fit models as those with the lowest AIC, and calculated pseudo R^2 with Nakagawa and Shielzeth's method for the model of the probability of local transmission and Cragg, Uhler, and Nagelkerke's method for remaining spatial models [58–61]. All regressions were conducted in R statistical software version 3.4.3 using the glm function in the base package.

Results

Epidemiological Data and tSIR Model

The duration and burden of Zika transmission and timing of epidemic peaks varied considerably both between and within countries (Figure 2). Within the countries included in this study, Zika emerged earliest in El Salvador in November of 2015, and latest in Colombia, which first reported a Zika case almost one year later in January of 2016 (Figure 2A). The weights for the serial interval were: $\omega_1 = 0.081, \omega_2 = 0.448; \omega_3 = 0.372; \omega_4 = 0.089; \omega_5 = 0.010$. Force of infection ranged from 0 to 15.409 cases per 100,000 people per week (model fit shown in Figure S3). In all countries there were weeks with no weekly local transmission ($\beta_t = 0$), but high case incidence resulting from imported cases. All countries included in our analyses had at least one province with local transmission (Figure 2B).

Spatiotemporal Model

The spatiotemporal hurdle model indicated that different climate factors were associated with the presence of weekly local transmission versus the intensity of weekly force of infection in a given province (Tables 1, S1-2). The best fit model for the presence of weekly local transmission included positive linear relationships with mean temperature and humidity and explained 3.7% of the variation in the likelihood of week to week transmission within provinces. The best fit model for the intensity of weekly force of infection included negative linear effects of mean temperature and humidity, as well as a positive linear effect of rainfall. This model explained 1.1% of the variation in the intensity of weekly force of infection. Alternative fixed effects models with month or month nested in province fixed effects produced similar results (Table S3-4).

Spatial Models

The spatial models indicated that geographic variation in epidemics was driven by climate and human population sizes (Figure 4, Tables S5-9). There was considerable geographic variation in Zika presence and intensity within and among countries in Latin America (e.g., Figure 3). We found a positive linear relationship between the presence of local transmission and humidity and mean temperature (Figure 4). For all other epidemic metrics, we found a unimodal relationship with mean temperature, although this relationship is not statistically significant in the models of cumulative cases and mean weekly cases (positive linear effect of mean temperature and negative quadratic effect of mean temperature; Figures 4-5). In provinces that had local transmission, mean force of infection peaked at 23.63°C (95% confidence interval: 22.20°C-25.49°C; Figure 5B). The population of the largest city had a positive relationship with

all epidemic characteristics aside from maximum force of infection (Figure 4). Mean humidity had a slight positive linear relationship with cumulative cases, while rainfall had a slight positive relationship with average weekly cases (Figure 4). All spatial models fit well based on their pseudo R^2 values (0.33-0.60) (Table 1).

Discussion

Climate and population factors were strong drivers of geographic variation in Zika epidemics, with different factors influencing where local transmission occurred compared with the intensity of transmission. Relative humidity, temperature, temperature range, and the population of the largest city were key determinants for whether local transmission occurred, and these factors could be used to determine regional likelihood for future *Aedes aegypti* transmitted diseases. Both the spatiotemporal and spatial models for the presence of local transmission included a positive linear effect of temperature, while the burden and intensity of epidemics (based on the other spatial models) included nonlinear effects of temperature (Table 1, Figure 4A). The large variation in epidemic characteristics across countries (Figures 2, 3A-B, 4) suggests that additional factors beyond climate and population size may also be important in driving Zika transmission. Understanding how climate drives different epidemic metrics is valuable for preparing for and responding to outbreaks. For example, the infrastructure and resources needed to respond to a large outbreak that spreads rapidly through the population, like what occurred in the Dominican Republic and El Salvador, are very different from what is needed to respond to an outbreak that affects fewer people at one time but lasts many months, as in Colombia and Guatemala.

Although climate strongly influenced spatial variation in Zika epidemic metrics, climate was not a strong predictor of Zika epidemic dynamics through time [22,29,37]. We hypothesize that week to week variation in transmission within provinces may be too stochastic to predict based on climate alone. For many of the provinces included in this study, climate rarely fell outside the suitable range for disease transmission, potentially indicating that given suitable climate conditions, non-climate factors such as reporting protocols, underlying immunity, transportation, and infrastructure may generate stochasticity that drives local temporal trends in Zika transmission. Another possible limitation in our ability to predict week to week variation in transmission could be due to errors in the epidemiological data, as suspected case numbers may differ considerably from laboratory-confirmed cases, and case reporting may change over time (e.g., as Zika awareness increases, people may become more likely to go to the doctor for a fever and doctors may be more likely to diagnose symptoms as Zika rather than another disease with similar symptoms such as dengue).

A surprising result of this study was the mismatch between the theoretically and empirically derived optimal temperature for Zika transmission and the temperatures we found to correspond with the greatest force of infection values during the 2015 to 2017 epidemic [25,62]. In previous studies, mechanistic R_0 models parameterized with data from laboratory experiments indicated that 29°C is optimal for Zika transmission [27,32]. However, our study demonstrated that the highest average force of infection values are found in provinces with mean temperatures between 20 and 26°C (Table 1), and laboratory studies confirm that Zika virus can be detected in the salivary glands of Aedes aegypti and transmitted at 25°C [63]. There are several possible hypotheses that could explain this discrepancy, including that: 1) provinces with mean temperatures around 29°C already implement vector control; 2) people may have acquired cross-

immunity from exposure to other arboviruses [25,64,65]; and/or 3) given suitable temperature for transmission, other factors that can covary with temperature such as land use, urbanization, and socioeconomics may be more important drivers of large epidemics [20].These hypotheses raise important questions about how to reconcile and ground truth theoretical and empirical studies with field data.

The 2015 to 2017 Zika outbreak provided an opportunity to investigate how population size and climate affect epidemic dynamics over time and space in a previously unexposed population. The results provide valuable insight into where Zika is likely to become endemic and how future outbreaks transmitted by *Aedes aegypti* could spread. Specifically, given that provinces with greater populations in their largest cities had longer and more intense outbreaks, regions with larger urban population sizes that also have suitable climate conditions for most of the year are most likely to sustain endemic Zika transmission. However, it is important to carefully consider how these results could apply to other regions, especially in places where Zika may be transmitted by other mosquito species, such as *Aedes africanus*, which exhibit different responses to climate [66]. Zika epidemics in Latin America were characteristically different across countries: some regions experienced large epidemics that spread quickly while others experienced low levels of sustained transmission (Figure 2). We would expect similar epidemic metrics to characterize other mosquito transmitted diseases that could emerge and re-emerge in the future, such as o'nyong nyong, Mayaro, and yellow fever [1,19,39–41]. Given this climate-driven geographic variation in epidemics, we would expect climate change to alter patterns in transmission for emerging and re-remerging mosquito-borne diseases in the future.

All data and code are accessible in a github repository: https://github.com/mrc-ide/ZikaModel.

Author contributions: EAM and JMC conceived of project; MH acquired data and conducted analyses; MH, JMC, and EAM interpreted data and wrote the manuscript.

Competing interests: All authors declare that there are no competing interests.

Funding: We received funding from a National Science Foundation (NSF) Ecology and Evolution of Infectious Diseases grant (DEB-1518681) and a Research Experiences for Undergraduates supplement, an NSF Grants for Rapid Response Research grant (RAPID 1640780), the Stanford University Woods Institute for the Environment Environmental Ventures Program, and the Hellman Faculty Fellowship.

348 References:

349 1. Gould E, Pettersson J, Higgs S, Charrel R, de Lamballerie X. 2017 Emerging arboviruses:
350 why today? *One Heal.* **4**, 1–13. (doi:10.1016/j.onehlt.2017.06.001)

351 2. Perkins TA, Metcalf CJE, Grenfell BT, Tatem AJ. 2015 Estimating drivers of
352 autochthonous transmission of chikungunya virus in its invasion of the Americas. *PLoS*
353 *Curr.* (doi:10.1371/currents.outbreaks.a4c7b6ac10e0420b1788c9767946d1fc)

354 3. Fritzell C, Rousset D, Adde A, Kazanji M, Van Kerkhove MD, Flamand C. 2018 Current
355 challenges and implications for dengue, chikungunya and Zika seroprevalence studies
356 worldwide: A scoping review. *PLoS Negl. Trop. Dis.* **12**, 1–29.
357 (doi:10.1371/journal.pntd.0006533)

358 4. Ali S *et al.* 2017 Environmental and social change explain the explosive emergence of
359 Zika virus in the Americas. *PLoS Negl. Trop. Dis.* **11**. (doi:10.1371/journal.pntd.0005135)

360 5. Pan American Health Organization / World Health Organization. 2018 Zika suspected and
361 confirmed cases reported by countries and territories in the Americas: Cumulative cases,
362 2015-2017. Updated as of 04 January 2018.

363 6. Finkenstädt BF, Grenfell BT. 2000 Time series modelling of childhood diseases: a
364 dynamical systems approach. *J. R. Stat. Soc. Ser. C* **49**, 187. (doi:10.1111/1467-
365 9876.00187)

366 7. Staples JE, Breiman RF, Powers AM. 2009 Chikungunya fever: an epidemiological
367 review of a re-emerging infectious disease. *Clin. Infect. Dis.* **49**, 942–948.
368 (doi:10.1086/605496)

369 8. Lardeux FJ, Tejerina RH, Quispe V, Chavez TK. 2008 A physiological time analysis of
370 the duration of the gonotrophic cycle of Anopheles pseudopunctipennis and its

371 implications for malaria transmission in Bolivia. *Malar. J.* **7**, 141. (doi:10.1186/1475-
372 2875-7-141)
373 9. Mordecai EA *et al.* 2013 Optimal temperature for malaria transmission is dramatically
374 lower than previously predicted. *Ecol. Lett.* **16**, 22–30. (doi:10.1111/ele.12015)
375 10. Grenfell BT, Bjorndstad ON, Kappey J. 2001 Travelling waves and spatial hierarchies in
376 measles epidemics. *Nature* **414**, 716. (doi:10.1038/414716a)
377 11. Reiner RC *et al.* 2014 Time-varying, serotype-specific force of infection of dengue virus.
378 *Proc. Natl. Acad. Sci.* **111**, e2694–e2702. (doi:10.1073/PNAS.1314933111)
379 12. French MD *et al.* 2015 Estimation of changes in the force of infection for intestinal and
380 urogenital schistosomiasis in countries with schistosomiasis control initiative-assisted
381 programmes. *Parasit. Vectors* **8**, 558. (doi:10.1186/s13071-015-1138-1)
382 13. Hafeez S, Amin M, Munir BA. 2017 Spatial mapping of temporal risk to improve
383 prevention measures: A case study of dengue epidemic in Lahore. *Spat. Spatiotemporal.*
384 *Epidemiol.* **21**, 77–85. (doi:10.1016/j.sste.2017.04.001)
385 14. Mueller I *et al.* 2012 Force of infection is key to understanding the epidemiology of
386 Plasmodium falciparum malaria in Papua New Guinean children. *Proc. Natl. Acad. Sci.*
387 **109**, 10030. (doi:10.1073/pnas.1200841109)
388 15. Pomeroy LW, Bjørnstad ON, Kim H, Jumbo SD, Abdoulkadiri S, Garabed R. 2015
389 Serotype-specific transmission and waning immunity of endemic foot-and-mouth disease
390 virus in Cameroon. *PLoS One* **10**. (doi:10.1371/journal.pone.0136642)
391 16. Carran S, Ferrari M, Reluga T. 2018 Unintended consequences and the paradox of control:
392 management of emerging pathogens with age-specific virulence. *PLoS Negl. Trop. Dis.*
393 **12**. (doi:10.1371/journal.pntd.0005997)

17. Egger JR, Ooi EE, Kelly DW, Woolhouse ME, Davies CR, Coleman PG. 2008 Reconstructing historical changes in the force of infection of dengue fever in Singapore: implications for surveillance and control. *Bull. World Health Organ.* **86**, 187. (doi:10.2471/blt.07.040170)

18. Gardner LM, Bóta A, Gangavarapu K, Kraemer MUG, Grubaugh ND. 2018 Inferring the risk factors behind the geographical spread and transmission of Zika in the Americas. *PLoS Negl. Trop. Dis.* **12**, 1–25.

19. Nah K, Mizumoto K, Miyamatsu Y, Yasuda Y, Kinoshita R, Nishiura H. 2016 Estimating risks of importation and local transmission of Zika virus infection. *PeerJ* **4**. (doi:10.1371/journal.pntd.0006194)

20. Mordecai EA *et al.* 2017 Detecting the impact of temperature on transmission of Zika, dengue, and chikungunya using mechanistic models. *PLoS Negl. Trop. Dis.* **11**. (doi:10.1371/journal.pntd.0005568)

21. Marcondes CB, Ximenes M de FF de M. 2015 Zika virus in Brazil and the danger of infestation by *Aedes (Stegomyia)* mosquitoes. *Rev. Soc. Bras. Med. Trop.* **49**, 4–10. (doi:10.1590/0037-8682-0220-2015)

22. Ryan SJ, McNally A, Johnson LR, Mordecai EA, Ben-Horin T, Paaijmans K, Lafferty KD. 2015 Mapping physiological suitability limits for malaria in Africa under climate change. *Vector Borne Zoonotic Dis.* **15**, 718–25. (doi:10.1089/vbz.2015.1822)

23. Costa EAPA, Santos EMM, Correia JC, Albuquerque CMR. 2010 Impact of small variations in temperature and humidity on the reproductive activity and survival of *Aedes aegypti* (Diptera, Culicidae). *Rev. Bras. Entomol.* **54**, 488–493. (doi:10.1590/S0085-56262010000300021)

417 24. Delatte H, Gimonneau G, Triboire A, Fontenille D. 2009 Influence of temperature on
418 immature development, survival, longevity, fecundity, and gonotrophic cycles of *Aedes*
419 *albopictus*, vector of chikungunya and dengue in the Indian Ocean. *J. Med. Entomol.* **46**,
420 33–41. (doi:10.1603/033.046.0105)
421 25. Tesla B, Demakovsky LR, Mordecai EA, Ryan SJ, Bonds MH, Ngonghala CN, Brindley
422 MA, Murdock CC. 2018 Temperature drives Zika virus transmission: evidence from
423 empirical and mathematical models. *Proc. R. Soc. B Biol. Sci.* **285**.
424 (doi:10.1098/rspb.2018.0795)
425 26. Eling W, Hooghof J, van de Vegte-Bolmer M, Sauerwein R, van Gemert G-J. 2001
426 Tropical temperatures can inhibit development of the human malaria parasite Plasmodium
427 falciparum in the mosquito. *Proc. Exper. Appl. Entomol* **12**, 151–156.
428 (doi:10.1073/pnas.1006422107)
429 27. Ciota AT, Matacchiero AC, Kilpatrick AM, Kramer LD. 2014 The effect of temperature
430 on life history traits of *Culex* mosquitoes. *J. Med. Entomol.* **51**, 55–62.
431 (doi:10.1603/ME13003)
432 28. Xiao FZ, Zhang Y, Deng YQ, He S, Xie HG, Zhou XN, Yan YS. 2014 The effect of
433 temperature on the extrinsic incubation period and infection rate of dengue virus serotype
434 2 infection in Aedes albopictus. *Arch. Virol.* **159**, 3053–3057. (doi:10.1007/s00705-014-
435 2051-1)
436 29. Brady OJ *et al.* 2014 Global temperature constraints on Aedes aegypti and Ae. albopictus
437 persistence and competence for dengue virus transmission. *Parasit. Vectors* **7**, 338.
438 (doi:10.1186/1756-3305-7-338)
439 30. Barton PS, Aberton JG, Kay BH. 2004 Spatial and temporal definition of *Ochlerotatus*

440 *camptorhynchus* (Thomson) (Diptera: Culicidae) in the Gippsland Lakes system of eastern
441 Victoria. *Aust. J. Entomol.* **43**, 16–22. (doi:10.1111/j.1440-6055.2004.00405.x)
442 31. Li CF, Lim TW, Han LL, Fang R. 1985 Rainfall, abundance of *Aedes aegypti* and dengue
443 infection in Selangor, Malaysia. *Southeast Asian J. Trop. Med. Public Health* **16**, 560–8.
444 32. Stewart-Ibarra AM, Lowe R. 2013 Climate and non-climate drivers of dengue epidemics
445 in southern coastal Ecuador. **88**, 971–981. (doi:10.4269/ajtmh.12-0478)
446 33. Morin CW, Monaghan AJ, Hayden MH, Barrera R, Ernst K. 2015 Meteorologically
447 driven simulations of dengue epidemics in San Juan, PR. *PLoS Negl. Trop. Dis.* **9**.
448 (doi:10.1371/journal.pntd.0004002)
449 34. Riou J, Poletto C, Boëlle PY. 2017 A comparative analysis of chikungunya and Zika
450 transmission. *Epidemics* **19**, 43–52. (doi:10.1016/j.epidem.2017.01.001)
451 35. Anyamba A *et al.* 2012 Climate teleconnections and recent patterns of human and animal
452 disease outbreaks. *PLoS Negl. Trop. Dis.* **6**. (doi:10.1371/journal.pntd.0001465)
453 36. Pontes RJ, Spielman A, Oliveira-Lima JW, Hodgson JC, Freeman J. 2000 Vector densities
454 that potentiate dengue outbreaks in a Brazilian city. *Am. J. Trop. Med. Hyg.* **62**, 378–383.
455 (doi:10.4269/ajtmh.2000.62.378)
456 37. Paaijmans KP, Wandago MO, Githeko AK, Takken W, Vulule J. 2007 Unexpected high
457 losses of Anopheles gambiae larvae due to rainfall. *PLoS One* **2**.
458 (doi:10.1371/journal.pone.0001146)
459 38. Koenraadt CJM, Harrington LC. 2008 Flushing effect of rain on container-inhabiting
460 mosquitoes *Aedes aegypti* and *Culex pipiens* (Diptera: Culicidae). *J. Med. Entomol.* **45**,
461 28–35. (doi:10.1603/0022-2585(2008)45[28:FEOROC]2.0.CO;2)
462 39. Wilder-Smith A, Gubler DJ, Weaver SC, Monath TP, Heymann DL, Scott TW. 2017

463 Epidemic arboviral diseases: priorities for research and public health. *Lancet. Infect. Dis.*
464 **17**, e101–e106. (doi:10.1016/S1473-3099(16)30518-7)
465 40. LaBeaud AD *et al.* 2015 High rates of o'nyong nyong and Chikuncunya virus
466 transmission in coastal Kenya. *PLoS Negl. Trop. Dis.* **9**.
467 (doi:10.1371/journal.pntd.0003436)
468 41. Wilder-Smith A, Monath TP. 2017 Responding to the threat of urban yellow fever
469 outbreaks. *Lancet. Infect. Dis.* **17**, 248–250. (doi:10.1016/S1473-3099(16)30588-6)
470 42. CDC Epidemic Prediction Initiative. In press. Zika Data Repository.
471 (doi:10.5281/zenodo.584136)
472 43. The Weather Company. In press. Weather Underground. See
473 https://www.wunderground.com/.
474 44. Bi P, Hiller JE, Cameron a S, Zhang Y, Givney R. 2009 Climate variability and Ross
475 River virus infections in Riverland, South Australia, 1992-2004. *Epidemiol. Infect.* **137**,
476 1486–93. (doi:10.1017/S0950268809002441)
477 45. Stewart Ibarra AM *et al.* 2013 Dengue vector dynamics (*Aedes aegypti*) influenced by
478 climate and social factors in Ecuador: implications for targeted control. *PLoS One* **8**,
479 e78263. (doi:10.1371/journal.pone.0078263)
480 46. Gharbi M, Quenel P, Gustave J, Cassadou S, La Ruche G, Girdary L, Marrama L. 2011
481 Time series analysis of dengue incidence in Guadeloupe, French West Indies: forecasting
482 models using climate variables as predictors. *BMC Infect. Dis.* **11**, 166.
483 (doi:10.1186/1471-2334-11-166)
484 47. Johansson MA, Dominici F, Glass GE. 2009 Local and global effects of climate on
485 dengue transmission in Puerto Rico. *PLoS Negl. Trop. Dis.* **3**.

(doi:10.1371/journal.pntd.0000382)

48. Laureano-Rosario AE, Garcia-Rejon JE, Gomez-Carro S, Farfan-Ale JA, Muller-Karger FE. 2017 Modelling dengue fever risk in the State of Yucatan, Mexico using regional-scale satellite-derived sea surface temperature. *Acta Trop.* **172**, 50–57. (doi:10.1016/j.actatropica.2017.04.017)

49. Brinkhoff T. In press. City Population.

50. Johansson MA, Powers AM, Pesik N, Cohen NJ, Staples JE. 2014 Nowcasting the spread of chikungunya virus in the Americas. *PLoS One* **9**. (doi:10.1371/journal.pone.0104915)

51. Faria NR *et al.* 2017 Establishment and cryptic transmission of Zika virus in Brazil and the Americas. *Nature* **546**, 406–410. (doi:10.1038/nature22401)

52. Ferguson NM, Cucunubá ZM, Dorigatti I, Nedjati-Gilani GL, Donnelly CA, Basáñez M-G, Nouvellet P, Lessler J. 2016 Countering the Zika epidemic in Latin America. *Science* **353**, 353–4. (doi:10.1126/science.aag0219)

53. Kraemer MUG, Perkins TA, Cummings DAT, Zakar R, Hay SI, Smith DL, Reiner RC, Jr. 2015 Big city, small world: density, contact rates, and transmission of dengue across Pakistan. *J. R. Soc. Interface* **12**. (doi:10.1098/rsif.2015.0468)

54. Perkins TA, Scott TW, Le Menach A, Smith DL. 2013 Heterogeneity, mixing, and the spatial scales of mosquito-borne pathogen transmission. *PLoS Comput. Biol.* **9**. (doi:10.1371/journal.pcbi.1003327)

55. Metcalf CJE, Munayco C V., Chowell G, Grenfell BT, Bjornstad ON. 2011 Rubella metapopulation dynamics and importance of spatial coupling to the risk of congenital rubella syndrome in Peru. *J. R. Soc. Interface* **8**, 369–376. (doi:10.1098/rsif.2010.0320)

56. Caudron Q, Mahmud AS, Metcalf CJE, Gottfrethsson M, Viboud C, Cliff AD, Grenfell

BT. 2014 Predictability in a highly stochastic system: final size of measles epidemics in small populations. *J. R. Soc. Interface* **12**. (doi:10.1098/rsif.2014.1125)

57. Croissant Y, Giovanni M. 2018 Panel Data Econometrics with R: the plm package.

58. Cragg JG, Uhler RS. 1970 The Demand for Automobiles. *Can. J. Econ. / Rev. Can. d'Economique* **3**, 386–406. (doi:10.2307/133656)

59. Nagelkerke NJD. 1991 A note on a general definition of the coefficient of determination. *Biometrika* **78**, 691–692. (doi:10.1093/biomet/78.3.691)

60. Nakagawa S, Schielzeth H. 2012 A general and simple method for obtaining R2 from generalized linear mixed-effects models. *Methods Ecol. Evol.* **4**, 133–142. (doi:10.1111/j.2041-210x.2012.00261.x)

61. McFadden D. 1975 Quantitative Methods for Analyzing Travel Behaviour of Individuals: Some Recent Developments. In *Behavioural travel modelling*, p. 35. North Holland Publishing Co.

62. Murdock CC, Evans M V., McClanahan TD, Miazgowicz KL, Tesla B. 2017 Fine-scale variation in microclimate across an urban landscape shapes variation in mosquito population dynamics and the potential of Aedes albopictus to transmit arboviral disease. *PLoS Negl. Trop. Dis.* **11**. (doi:10.1371/journal.pntd.0005640)

63. Hernández-Triana LM *et al.* 2019 Evidence for infection but not transmission of Zika virus by Aedes albopictus (Diptera: Culicidae) from Spain. *Parasit. Vectors* **12**, 204. (doi:10.1186/s13071-019-3467-y)

64. Gething PW, Smith DL, Patil AP, Tatem AJ, Snow RW, Hay SI. 2010 Climate change and the global malaria recession. *Nature* **465**, 342–345. (doi:10.1038/nature09098)

65. Wen J, Elong Ngono A, Regla-Nava JA, Kim K, Gorman MJ, Diamond MS, Shresta S.

532 2017 Dengue virus-reactive CD8+ T cells mediate cross-protection against subsequent
533 Zika virus challenge. *Nat. Commun.* **8**, 1459. (doi:10.1038/s41467-017-01669-z)
534 66. Vorou R. 2016 Zika virus, vectors, reservoirs, amplifying hosts, and their potential to
535 spread worldwide: what we know and what we should investigate urgently. *Int. J. Infect.*
536 *Dis.* **48**, 85–90. (doi:https://doi.org/10.1016/j.ijid.2016.05.014)
537

Tables

Table 1: Response variables for the spatiotemporal (ST) and spatial (S) models, with their corresponding thermal optima. R^2 values were calculated for the spatiotemporal models and pseudo R^2 values were calculated for the spatial models using Nakagawa's pseudo R^2 for the mixed effect local transmission model (which produces a marginal and conditional pseudo R^2) and Nagelkerke's pseudo R^2 for the other spatial models. For the best fit models, temperature and humidity correspond to mean temperature and mean humidity over a three-week period, lagged by six weeks from the week of case reporting. Temperature^2 corresponds to squared temperature over a three-week period, lagged by six weeks from the week of case reporting. Rainfall corresponds to cumulative rainfall over a six-week period, lagged by three weeks from the week of case reporting. In the case of the spatial models, climate covariates are averaged over the course of the epidemiological data and city pop corresponds to the population of each province's largest city.

Response variable	**Description**	**Model Type**	**Thermal Optimum (°C)**	**R^2/ Pseudo R^2**	**Sample Size**	**Best Fit Model**
Weekly Local Transmission	The likelihood that β_t exceeded zero for a given week	ST	N/A	0.037	7,109	$P(\beta_t>0)$ ~ ~0.07 × temperature +0.06 × humidity
Intensity of Weekly Force of Infection	The magnitude of $ln(\beta_t)$, given that it exceeded one	ST	N/A	0.011	2,031	$ln(\beta_t)$ ~ 0.07 × temperature - 0.08 × humidity + 0.04 × rainfall
Local Transmission	The likelihood that β_t exceeded zero for any week	S	N/A	Marginal: 0.281 Conditional: 0.599	127	P(local trans) ~ 0.49 × temperature + 1.15 × humidity - 0.07 × rainfall + 0.82 × city pop
Maximum Force of Infection	Logged maximum value for β_t in provinces with local transmission	S	23.93 (95% CI: 22.02-26.90)	0.534	114	ln(max(β_t)) ~ - 2.30 × temperature^2 + 2.44 × temperature
Mean Force of Infection	Logged mean value for β_t in provinces with local transmission	S	23.63 (95% CI: 22.20-25.49)	0.596	114	ln(mean(β_t)) ~ - 2.78 × temperature^2 + 2.75 × temperature + 0.19 × city pop
Cumulative Cases	Total number of cases reported	S	22.51 (95% CI: 20.57-30.68)	0.330	127	cumulative cases ~ - 1.68 × temperature^2 + 1.69 × temperature + 0.16 × humidity + 0.21 × city pop
Mean Weekly Cases	Mean number of cases in weeks with any cases reported	S	23.69 (95% conf: 19.57-26.12)	0.348	127	mean weekly cases ~ - 1.59× temperature^2 + 1.69 × temperature + 0.14 × rainfall + 0.35 × city pop

Figure Captions

Figure 1: Illustration of epidemic metrics that characterize the presence, burden, and intensity of outbreaks. (A) Cartoon of weekly incidence during an outbreak where cumulative cases are calculated by taking the sum of all cases across all weeks during the outbreak, and mean cases (dashed horizontal line) are calculated as the mean of all cases in weeks with at least one case during the outbreak. (B) Cartoon of logged weekly force of infection during an outbreak where the highest value corresponds to maximum force of infection and the dashed horizontal line corresponds to the mean force of infection.

Figure 2: Heatmaps of weekly case incidence and force of infection. Each row corresponds to a single province over time, with lines separating the following countries: DOM = Dominican Republic, SLV = El Salvador, COL = Colombia, ECU = Ecuador, MEX = Mexico, GTM = Guatemala. Gray shading indicates no available data. The color represents (A) weekly logged cases for each province and (B) logged force of infection. Red indicates high values and blue indicates low values. White indicates (A) no cases reported or (B) no presence of local transmission (β_t=0) in a given week.

Figure 3: Geographic differences in epidemic metrics. Provinces are colored by (A) whether local Zika transmission was present (red) or absent (blue); (B) logged mean force of infection; and (C) mean temperature. Provinces that we excluded from this study due to lack of epidemiological or climate data (see Methods) are white. Countries not included in this study are grey.

Figure 4: Coefficients for factors driving geographic differences in epidemics. Plots display coefficients included in the best fit spatial model for presence local transmission (lavender), maximum force of infection (blue), mean force of infection (green), cumulative cases (olive),

590 and mean weekly cases (salmon). Points and horizontal lines indicate the mean coefficient values
591 and 95% confidence intervals, respectively. Note that the presence of local transmission model is
592 excluded from the panels reporting country fixed effects, as this model incorporates a random
593 effect of country.

594 **Figure 5: Nonlinear relationship between temperature and epidemic characteristics.** Plots
595 showing the relationship between mean temperature and (A) logged maximum force of infection
596 and (B) logged mean force of infection. The model prediction is indicated by the blue lines, and
597 the 95% confidence interval is indicated by the red dashed lines. The gray shaded region
598 indicates the 95% confidence interval for the thermal optimum. The F-statistic for the nonlinear
599 effect of temperature and its p-value are given in the inset. The response variables are scaled to
600 be between zero and one.

601

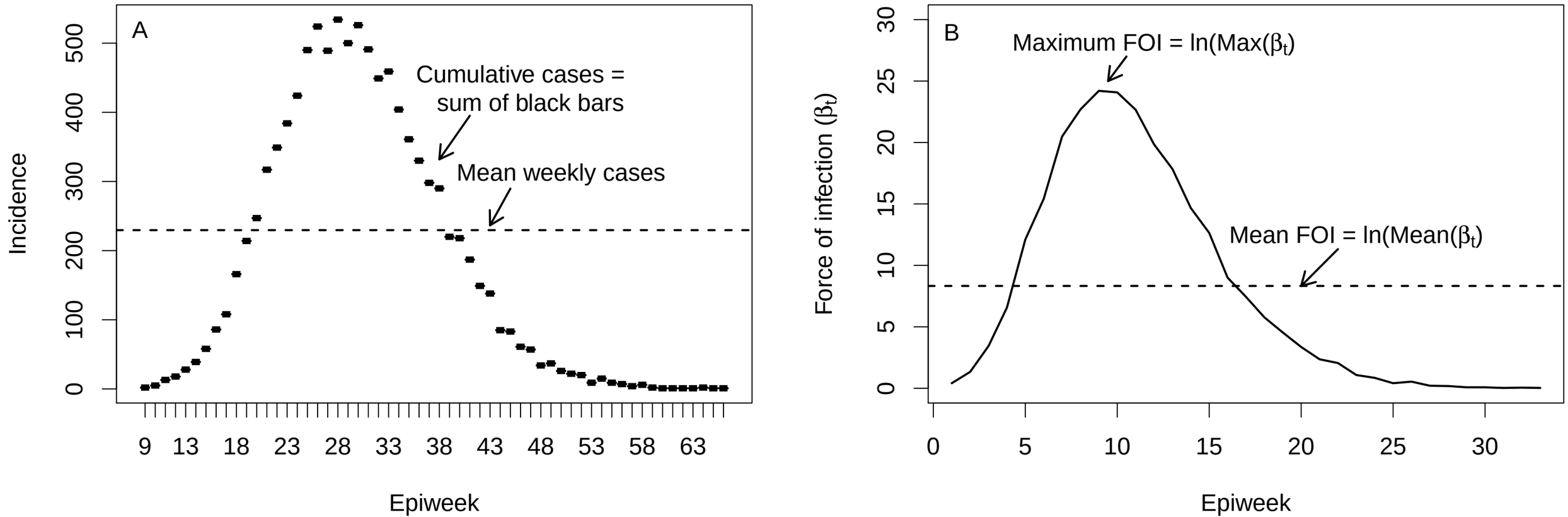
A
Cumulative cases =
sum of black bars
Mean weekly cases
Incidence
0
100
200
300
400
500
9
13
18
23
28
33
38
43
48
53
58
63
Epiweek
B
Maximum FOI = ln(Max(βt)
Mean FOI = ln(Mean(βt)
Force of infection (βt)
0
5
10
15
20
25
30
Epiweek

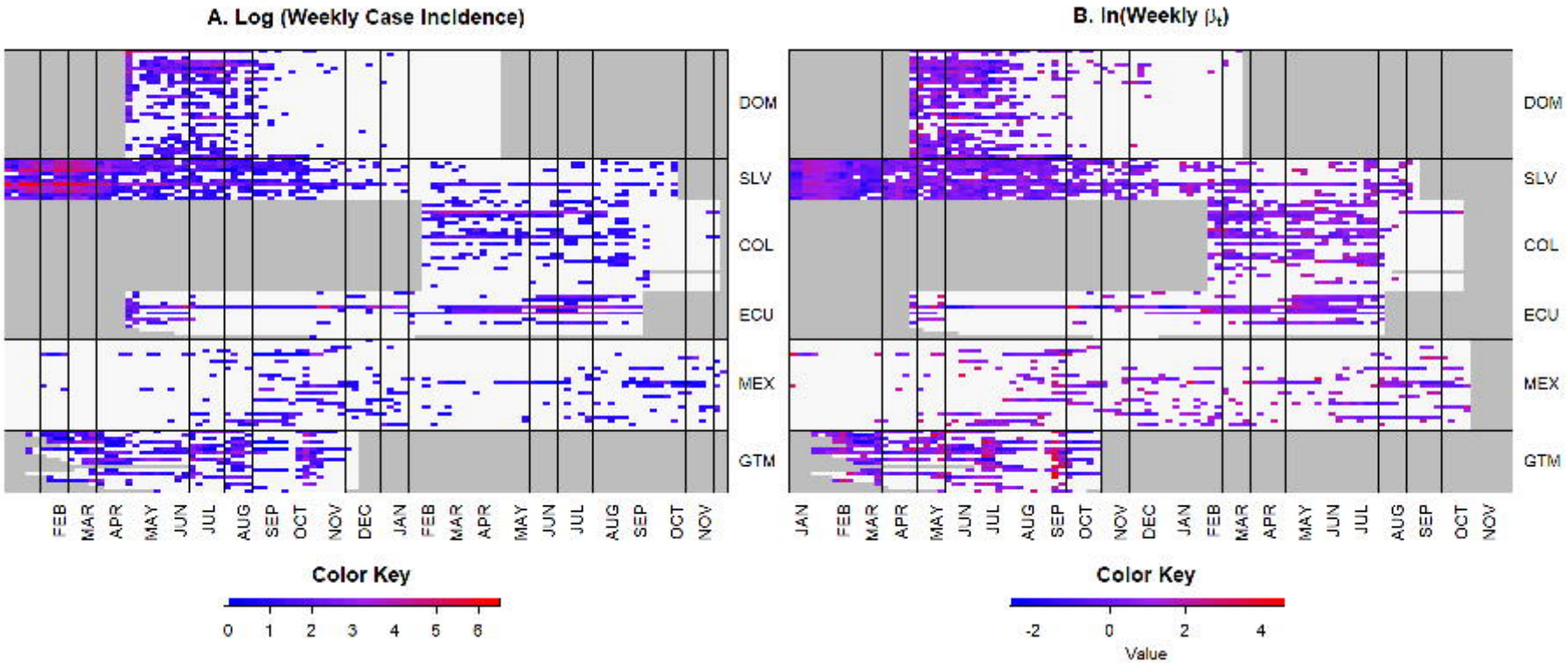
A. Log (Weekly Case Incidence)
B. ln(Weekly β_t)
DOM
SLV
COL
ECU
MEX
GTM
FEB MAR APR MAY JUN JUL AUG SEP OCT NOV DEC JAN FEB MAR APR MAY JUN JUL AUG SEP OCT NOV
JAN FEB MAR APR MAY JUN JUL AUG SEP OCT NOV DEC JAN FEB MAR APR MAY JUN JUL AUG SEP OCT NOV
Color Key
0 1 2 3 4 5 6
Color Key
-2 0 2 4
Value

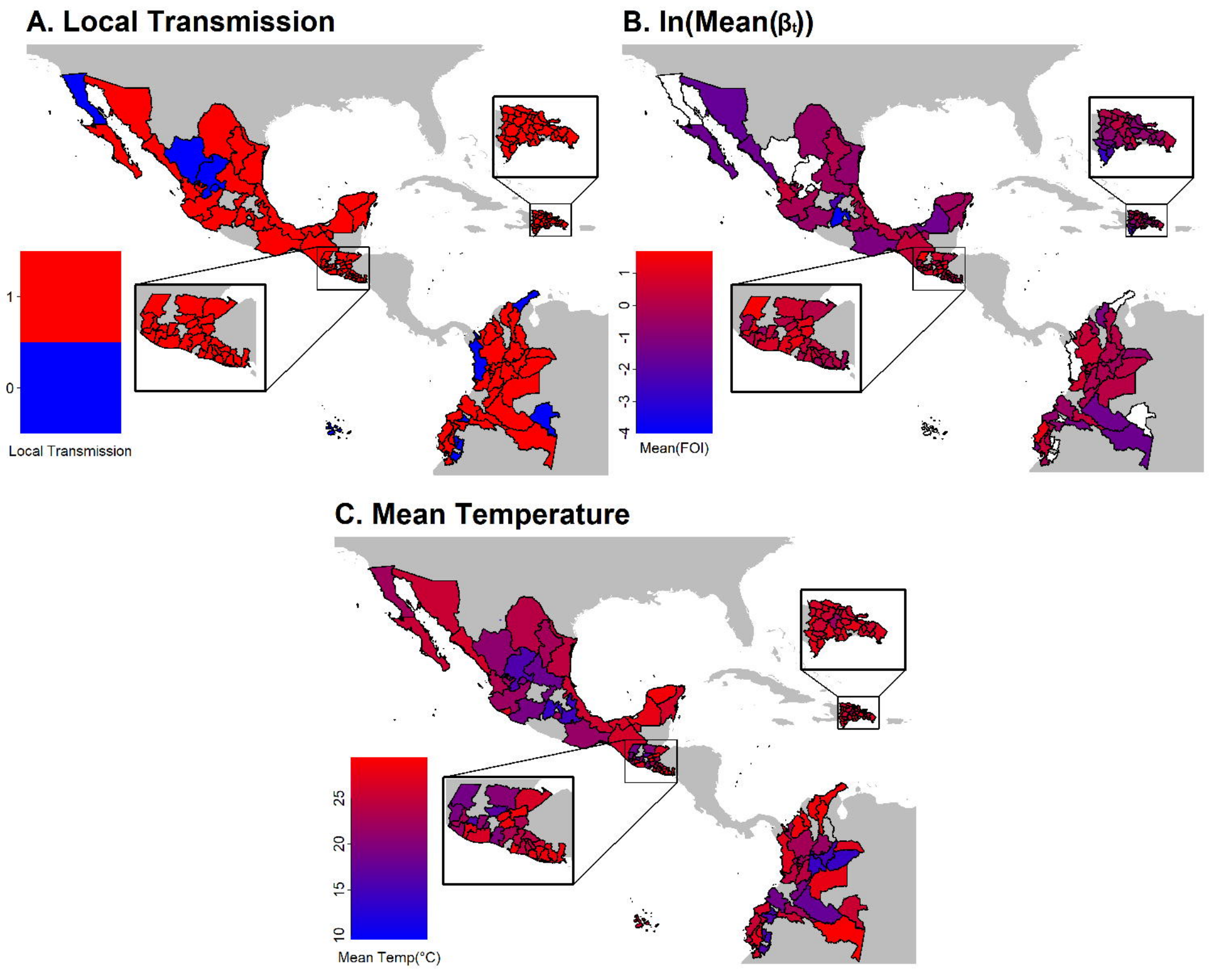
A. Local Transmission
1
0
Local Transmission
B. ln(Mean(βt))
1
0
-1
-2
-3
-4
Mean(FOI)
C. Mean Temperature
25
20
15
10
Mean Temp(°C)

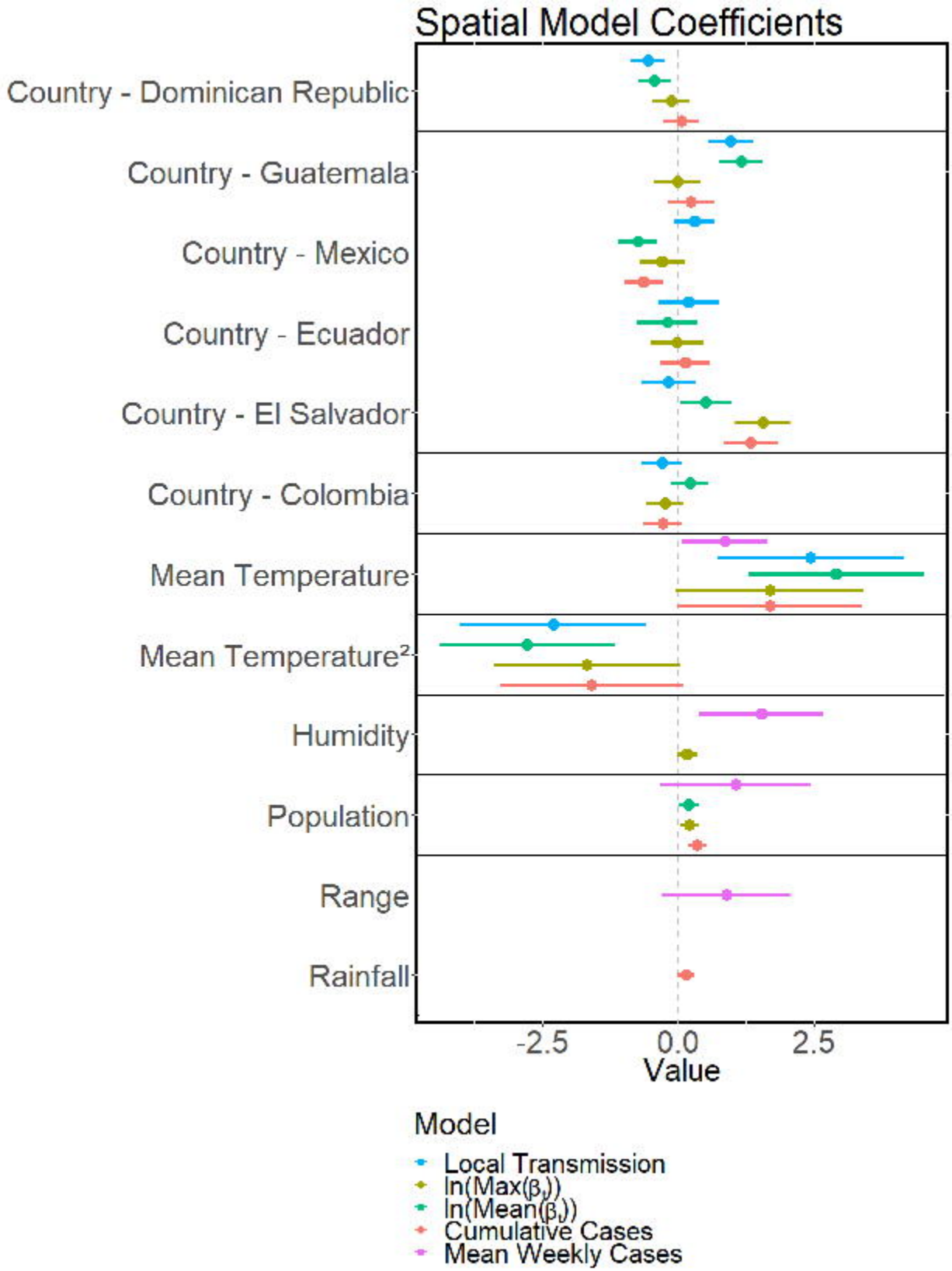
Spatial Model Coefficients
Country - Dominican Republic
Country - Guatemala
Country - Mexico
Country - Ecuador
Country - El Salvador
Country - Colombia
Mean Temperature
Mean Temperature²
Humidity
Population
Range
Rainfall
-2.5
0.0
2.5
Value
Model
Local Transmission
ln(Max(β_i))
ln(Mean(β_i))
Cumulative Cases
Mean Weekly Cases

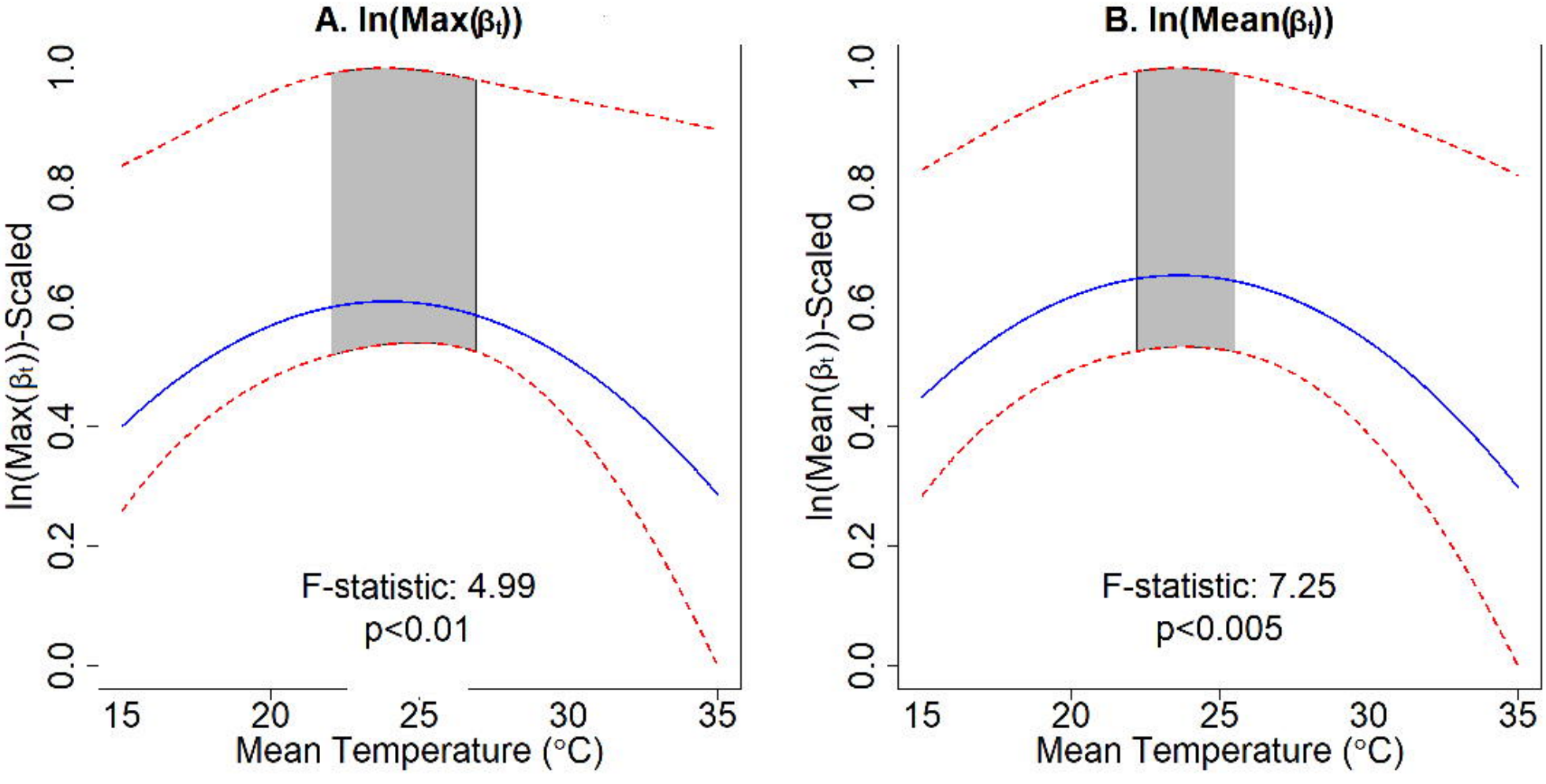
A. ln(Max(βt))
ln(Max(βt))-Scaled
0.0
0.2
0.4
0.6
0.8
1.0
F-statistic: 4.99
p<0.01
15
20
25
30
35
Mean Temperature (°C)
B. ln(Mean(βt))
ln(Mean(βt))-Scaled
0.0
0.2
0.4
0.6
0.8
1.0
F-statistic: 7.25
p<0.005
15
20
25
30
35
Mean Temperature (°C)